

# Comparison of dual energy CT and two channel spectral CT to predict proton stopping powers for proton therapy planning

Maarten Diepeveen (S2711362)



**rijksuniversiteit  
groningen**

A thesis submitted in partial fulfillment for the  
degree of Bachelor of Science

in the

Faculty of Science and Engineering  
University of Groningen

Supervisors:

dr. E.R. van der Graaf

dr. P.G. Dendooven

July 2018

# Contents

<b>1</b>	<b>Introduction</b>	<b>3</b>
<b>2</b>	<b>Theory</b>	<b>5</b>
2.1	CT scans . . . . .	5
2.1.1	Single energy Computed Tomography . . . . .	5
2.1.2	Multi-Energy CT . . . . .	6
2.2	Linear attenuation coefficient . . . . .	8
2.3	HU values . . . . .	9
2.4	True stopping powers . . . . .	9
2.5	Effective atomic number . . . . .	10
2.6	Stopping power for dual CT and spectral CT . . . . .	10
<b>3</b>	<b>Materials and methods</b>	<b>11</b>
<b>4</b>	<b>Results</b>	<b>13</b>
4.1	HU Values . . . . .	13
4.2	Linear attenuation coefficient . . . . .	13
4.3	True stopping power . . . . .	16
4.4	Effective atomic number . . . . .	16
4.5	Mean excitation energy . . . . .	22
4.6	Stopping power . . . . .	23
<b>5</b>	<b>Discussion and conclusion</b>	<b>25</b>

# 1 Introduction

Proton therapy is a technique which can be used to treat cancer patients. It uses protons to irradiate the tumor instead of photons or electrons which are used in standard radiotherapy. It has a lot of advantages over other types of radiotherapy of which the biggest advantage is that more accurate dose distributions can be delivered. This allows a better targeting of the tumor and less damage to the healthy tissue. Every tumor can be destroyed with radiation the problem however, is that also healthy tissue is exposed which may result in damage or secondary tumors. Therefore the goal of radiation therapy is to get the prescribed dose in the tumor and to minimize the dose in the healthy tissues. Protons have a very rapid energy loss in the last few millimeters of penetration. This results in a very sharp peak in the dose distribution known as the Bragg peak. When a proton moves through matter the ionization energy is inversely proportional to the square of the velocity. This explains the sharp peak occurring just before the particle completely stops. The penetration depth of the proton and therefore of the Bragg peak is directly related to the initial energy of the proton. The desired dose can be placed anywhere in the patient. A proton beam can therefore achieve significant dose reduction in comparison to a photon beam.

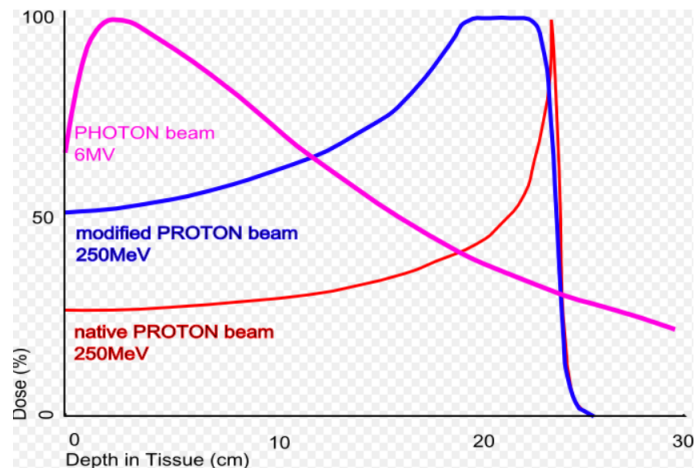


Figure 1: The pink line is the photon beam, these photons are created using a LINAC. The voltage at which the electrons are accelerated is  $V=6\text{MV}$ , this causes the highest possible energy for the electrons to be  $E=6\text{MeV}$ . The red line is the proton beam with protons of energy  $E=250\text{MeV}$ . The blue line is the modified proton beam, the original mono-energetic proton beam (red line) is widened by using a range of energies. This widened beam is called the spread out Bragg peak[1].

In figure 1 the dose in percentages is plotted against the depth in tissue in centimeters both for a proton beam and a photon beam. The photon beam is

generated by a linear accelerator (LINAC) which accelerates electrons or other charged particles by oscillating electric potentials. After the electrons reach a certain speed they hit a target to slow them down[2]. Due to this loss of energy the electrons produce radiation, this process is called Bremsstrahlung. Here one can clearly see how the dose distribution of a proton beam is superior to the dose distribution of the photon beam[3].

For the planning of proton therapy different scans are made of the human body. These scans do not only have to give information about the location of the tumor, but also which tissues are in the radiation path. A proton is slowed down in its path and therefore the tissue through which the proton travels must be known in order to know the degree in which it is slowed down. The extent in which a material stops the proton is called the proton stopping power of the material. This stopping power must be known very accurately to estimate the proton range and consequently get the prescribed dose in the tumor and not in the healthy tissue.

These scans can be done by using dual energy CT scan or by a spectral CT. The CT scan, which stands for computed tomography scan, uses X-rays to make images of inside the body. The CT scan virtually divides the body up into voxels, this allows the user to see inside the body. A voxel represents a value on a three dimensional grid. It is actually a three dimensional pixel[4]. The X-rays in the CT scan are created by X-ray tubes, an X-ray tube converts electricity into X-rays. A high speed electron hits a metal target, when the electron collides with electrons in the metal it decelerates. As it decelerates the energy the electron loses is converted into X-rays[5]. A dual CT scan uses a low voltage and a high voltage for the X-ray tubes, in this research a low voltage of 90kV is used and a high voltage of 150kV (Sn) filtered by a few millimeters of tin is used. For the spectral CT the voltage of the tube is set to 120kV. Spectral CT uses an energy sensitive detector such that on the transmission side an energy spectrum can be measured. Due to this two or more energy channels can be created. These X-rays give us information about the linear attenuation coefficient of every voxel. The linear attenuation coefficient characterizes how easily every voxel can be penetrated by the X-ray. A large linear attenuation coefficient means that the intensity of the X-ray is relatively strongly attenuated when traveling through this voxel, a smaller linear attenuation coefficient means that the X-ray is less attenuated. The unit of the linear attenuation coefficient is in reciprocal metre ( $m^{-1}$ )[6]. With this linear attenuation coefficient Hounsfield units (HU values) can be calculated. A HU value is a linear transformation of the linear attenuation coefficient relative to the linear attenuation coefficient of water[7]. HU values are scaled such that water has a HU value of 0 and air has an HU value of -1000. In figure 2 one can see a CT scan of the abdomen with the indicated HU values. The spine is shown down below and has relatively high HU values, this is due to the high density of bone. The lung is shown left and right of the spine and also the HU value of air in the lung is displayed. This is the value -798 which is relatively close to the HU value of true air of -1000.

The goal of this research is to see how the stopping powers estimated by dual energy CT relate to the stopping powers estimated by spectral energy CT.

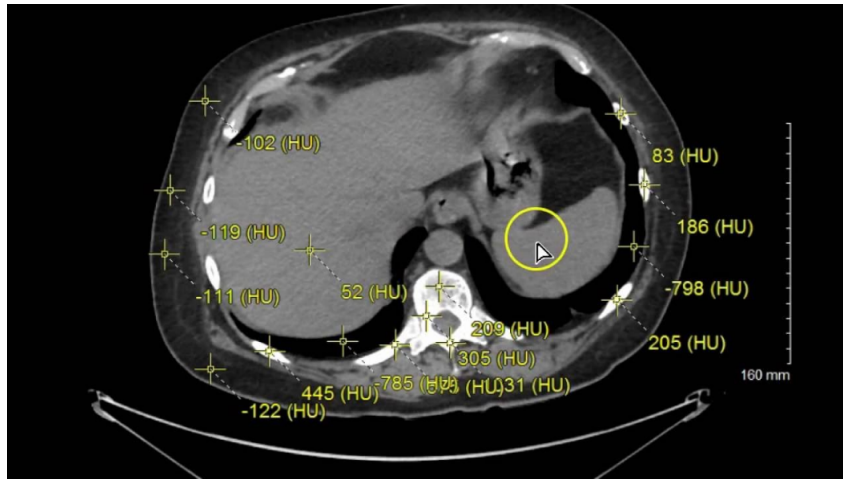


Figure 2: CT scan of the abdomen with indicated HU values[8].

Especially how to stopping power changes when the energy window of spectral CT are varied. These stopping powers are also compared to the true stopping powers, which are known for the materials used.

## 2 Theory

### 2.1 CT scans

#### 2.1.1 Single energy Computed Tomography

A single energy CT (SECT) makes cross-sectional images of the human body by using intensity profiles of a photon beam (X-rays). These images are made by an X-ray tube and an opposing detection system which is rotating around the patient as can be seen in figure 3.

CT scans divide the patient up into voxels. The detector measures the intensity of the X-ray after passing through the patient and then convert this to an digital number which is set to a certain voxel. With these values a linear attenuation coefficient can be derived and also the HU values can be determined which is both explained later on[4].

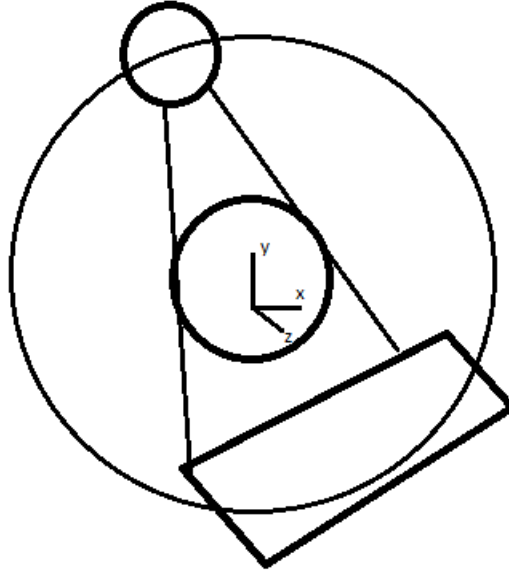


Figure 3: CT scan of the body, the circle on top is the X-ray tube where the X-rays are generated. The square on the bottom is the detector.

### 2.1.2 Multi-Energy CT

Dual energy CT (DECT) refers to a CT that uses two different X-ray tube voltages. This is shown in figure 4. The form of dual energy CT which is used is dual source dual energy CT. Dual source DECT uses two X-ray tubes at different voltages, a low voltage and a high voltage and two detectors on the opposite sites of the X-ray tubes. In this research a low voltage of 90keV is used and a high voltage of 120keV[9]. The energy spectrum of dual CT is shown in figure 5. The red line is the energy spectrum for 90kV and the green line is the energy spectrum for 150(Sn)kV.

Spectral energy CT uses one X-ray tube voltage instead of two as the dual energy CT does, in this research of 120keV. In spectral CT one can set two or more channels on the transmission side at the detector. In these channels certain windows can be chosen such that the detector measures in this energy spectrum. In figure 6 the energy spectrum of spectral CT is shown. The two channels are also drawn in the figure ranging from 30keV till 70keV and from 70keV till 120keV.

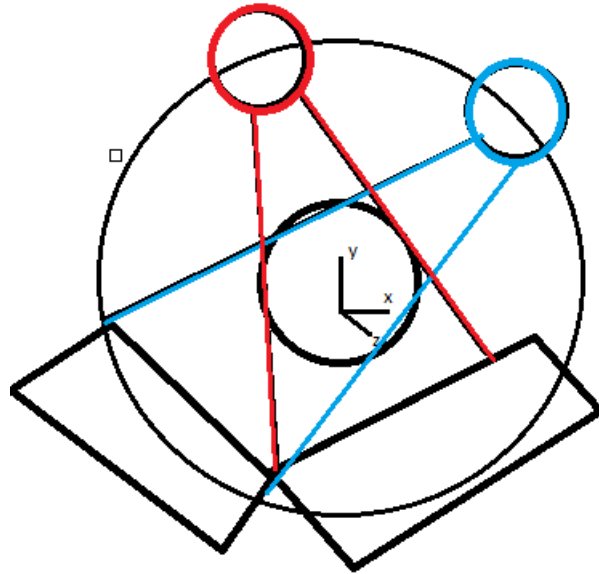


Figure 4: Dual CT scan, the circles on top are the X-ray tubes where the X-rays are generated and the squares on the bottom are the detectors.

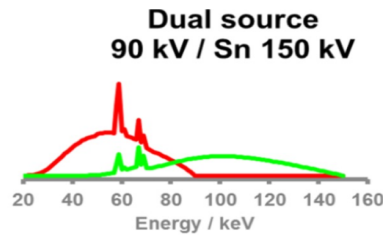


Figure 5: DECT energy spectrum of 90kV(red) and 150(Sn)kV(green)[10].

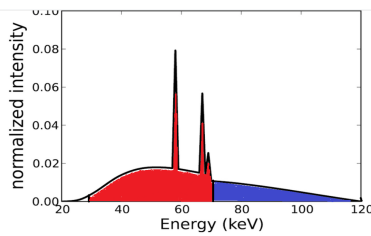


Figure 6: Spectral CT with a tube voltage of 120keV and two channels ranging from [30,70]keV and [70,120]keV. The high energy window is drawn in blue and the low energy window is drawn in red[11]

## 2.2 Linear attenuation coefficient

The linear attenuation coefficient characterizes how easily a volume can be penetrated and is defined by formula 1

$$I = I_0 e^{-\mu x} \quad (1)$$

It describes how many X-rays are absorbed or scattered per meter the X-rays travelled through the tissue.  $I$  denotes the intensity of the photons across a distance  $x$  and has unit  $W/cm^2$ ,  $I_0$  is the initial intensity of the photon and is also given in  $W/cm^2$ ,  $\mu$  is the linear attenuation coefficient in  $cm^{-1}$  and  $x$  is the distance traveled in m. In figure 7 the linear attenuation coefficient of six different materials is plotted against the energy.

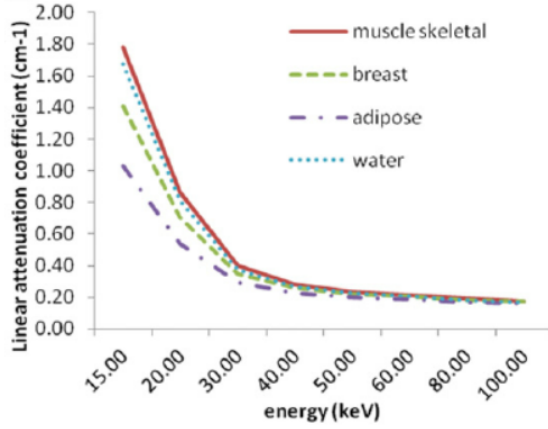


Figure 7: Linear attenuation coefficient vs energy for different tissues and water[12].

The linear attenuation coefficient in terms of electron density and total electronics cross section is given by the formula

$$\mu(E) = \rho_e \sigma^{tot}(E, Z') \quad (2)$$

Where  $\rho_e$  is the electron density in electrons per  $cm^3$  and  $\sigma^{tot}(E, Z')$  is the total electronic cross section in  $cm^2$  which depends on the energy in eV.  $Z'$  is the effective atomic number. Every atom has its own atomic number, the effective number  $Z'$  is the average atomic number of a composition. The electron density is given by

$$\rho_e = \rho N_g = \rho N_A \sum w_k \frac{Z_k}{A_k} \quad (3)$$

Where  $\rho$  is the mass density in  $g/cm^3$ , the  $N_A$  is the number of Avogadro and is given by  $N_A = 6.022 * 10^{23} \text{ mol}^{-1}$ ,  $w_k$  is the mass fraction of element k,  $Z_k$  is the atomic number of element k and  $A_k$  is the atomic mass number of element k[13].

### 2.3 HU values

HU values form a scale which also characterizes how easily a material is penetrated just as the linear attenuation coefficient. It is a linear transformation of the linear attenuation coefficient relative to the linear attenuation coefficient of water. It is defined such that the HU value of distilled water at standard pressure and temperature (STP) is zero and the HU value of air at STP is equal to -1000 HU. For the calculation of the HU values the following formula is used

$$H = \frac{(\mu - \mu^w)}{\mu^w} * 1000 \quad (4)$$

Here the  $\mu$  is the attenuation coefficient in  $\text{cm}^{-1}$  of the material in question, the  $\mu^w$  is the attenuation coefficient of water and is also in  $\text{cm}^{-1}$ .

Now before the HU values can be calculated the attenuation coefficient needs to be multiplied with a function  $\Omega(E)$ .

$$\mu_j = \int_0^\infty \Omega(E)\mu(E)dE \quad (5)$$

Where the  $\mu(E)$  is the linear attenuation coefficient calculated as mentioned before and  $\Omega(E)$  is a system weighting function. The system weighting function is a convolution of the spectrum of the X-ray tubes of the CT scan and the detector response.

### 2.4 True stopping powers

The stopping power describes the force which acts on charged particles which travel through matter[14]. This stopping power results in loss of the particle's energy. The proton stopping power is defined as

$$-\frac{dE}{dx} = \frac{4\pi k_0^2 e^4 \rho_e}{mc^2 \beta^2} \ln \frac{2mc^2 \beta^2}{I(1 - \beta^2)} - \beta^2 \quad (6)$$

In this relation  $k_0$  is a constant defined as  $k_0^2 = 3.16 * 10^{45} \text{ MeV}^2 m^2 C^{-4}$ ,  $e$  is the electron charge  $e^4 = 6.5536 * 10^{-76} \text{ C}^{-4}$ ,  $\rho_e$  is the electron density in electrons per  $\text{m}^3$ ,  $mc^2$  is the rest mass of an electron multiplied with the light speed  $c$  and is equal to  $mc^2 = 0.511 \text{ MeV}$ ,  $\beta$  is the speed of the particle relative to the light speed and is defined as

$$\beta = v/c \quad (7)$$

Where  $v$  is the speed of the proton for a proton of 219MeV, the 219MeV is chosen as an average proton energy which gives a value of  $\beta^2 = 0.343$ . The  $I$  is the mean excitation energy of the medium in MeV. The mean excitation energy of the medium is given by

$$\ln \langle I \rangle = \frac{\sum w_k \frac{Z_k}{A_k} \ln(I_k)}{\sum w_k \frac{Z_k}{A_k}} \quad (8)$$

The medium is a combination of different elements  $k$ . Here  $\ln(I_k)$  is the mean excitation energy of element  $k$  in the medium in MeV. The sample materials for which the stopping power is calculated are certain plastics with HU values close to the body tissues which they represent. The properties of these sample materials such as the density and the composition are known, because all these properties are known the true stopping power can be calculated[15].

## 2.5 Effective atomic number

The effective atomic number is the average atomic number for a mixture of materials. For most of the interaction properties it is useful to define an effective atomic number for the compound. By measuring two different attenuation coefficients the effective atomic number  $Z'$  can be calculated by using the following relationship

$$\frac{\mu_H}{\mu_L} = \frac{\int_0^\infty w_H(E)(e\sigma^{tot}(E, Z'))dE}{\int_0^\infty w_L(E)(e\sigma^{tot}(E, Z'))dE} \quad (9)$$

When solving this equation the effective atomic number  $Z'$  for a compound or mixture from the  $Z$  dependence can be found. The numerator and denominator originates from equation 5. The  $w_H$  and  $w_L$  are system weighting functions(SWF) for the high energy spectral distribution and low energy spectral distribution respectively. The system weighing function is defined as

$$w(E) = \frac{S(E)D(E)}{\int_0^\infty S(E)D(E)dE} \quad (10)$$

Where  $S(E)$  source output after tube filtration and  $D(E)$  is the detector efficiency. With this  $Z'$  the electron density  $\rho_e$  can be calculated with only one value for  $\mu$  [13].

## 2.6 Stopping power for dual CT and spectral CT

Now with the true stopping power known the stopping power is calculated for the dual CT scan and the spectral CT scan. To calculate this the effective atomic number  $Z'$  is linked to the mean excitation energy ( $I$ ) with a relatively smooth cubic function.

$$\frac{\ln(I)}{Z'} = cZ'^3 + dZ'^2 + fZ' + g \quad (11)$$

The coefficients in this relation depend on the energies used in the DECT scan, this is due to the fact that the effective atomic number depends on the x-ray energies. The third order polynomial of equation 11 is shown in figure 8.

The effective atomic number  $Z'$  is calculated from the composition, the density and the SWF. The values for carbon, teflon, aluminum and  $Al_2O_3$  may deviate a bit from the curve due to the fact that there is almost no hydrogen in the composition[16]. Mean excitation energies have been calculated for 39 materials which are described later on using formula 8. A relationship is now

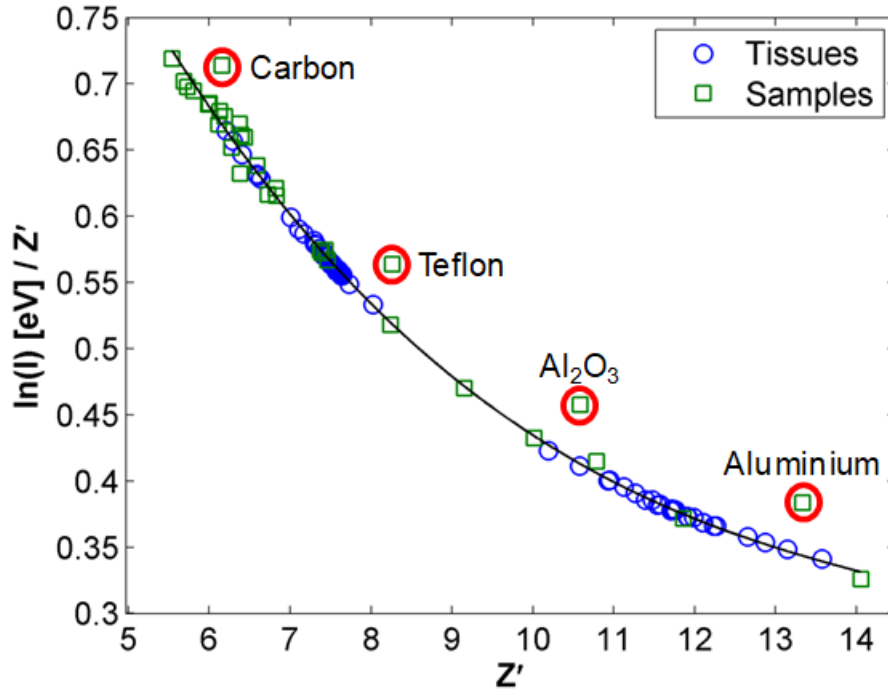


Figure 8: Ratio of  $\ln(I)/Z'$  vs the  $Z'$  for 80 different tissues described by Woodard and White[16] and  $\ln(I)/Z'$  vs  $Z'_{calculated}$  for 32 sample materials[13].

found, the least squares fitted values of the free parameters are  $c = -2.655 \cdot 10^{-4}$ ,  $d = 1.252 \cdot 10^{-2}$ ,  $f = -2.103 \cdot 10^{-1}$  and  $g = 1.551$ [13].

### 3 Materials and methods

The goal of this research is to find an optimum set of windows for spectral energy to get the best approximation of the stopping power. The low energy tube voltage of DECT is 90keV and the high energy tube voltage of DECT is 150(Sn)keV. The energy tube voltage of spectral CT is 120 keV, with a low window of which starts with a spectrum of [30,70]keV and a high spectrum of [70,120]keV. Then a separation is introduced in the window which increases in increments of 5, so the next spectrum has a low energy spectrum of [30,67]keV and a high energy spectrum of [72,120]keV all the way up to a low energy spectrum of [30,35]keV and a high energy spectrum of [105,120]keV. So the linear attenuation coefficient is calculated for 39 different materials and for every energy window, the materials are given in the table 1. Now with the

linear attenuation coefficient the HU values are calculated for all the sample materials and for every window of the spectral energy. The  $HU_H/HU_L$  is then plotted against the separation, also the linear attenuation coefficient  $\mu_H/\mu_L$  is plotted against the separation.

Table 1: Table of all materials used with their chemical formula.

Material used			
Material	Ch. formula	Material	Ch. formula
LN-300 lung		LN-450 lung	
AP6 adipose		BR12 breast	
CT SW solid water		Solid water M457	
Aluminum	AlMgSi1	BRN-SR2 brain	
LV1 liver		IB3 inner bone	
B200 bone mineral		CB2-30%	CaCO <sub>3</sub>
CB2-50%	CaCO <sub>3</sub>	SB3 cortical bone	
n-Pentane	C <sub>5</sub> H <sub>12</sub>	n-Hexane	C <sub>6</sub> H <sub>14</sub>
n-Heptane	C <sub>7</sub> H <sub>16</sub>	Methanol	CH <sub>4</sub> O
Ethanol	C <sub>2</sub> H <sub>6</sub> O	Propan-1-ol	C <sub>3</sub> H <sub>8</sub> O
Propan-2-ol	C <sub>3</sub> H <sub>8</sub> O	Oleic acid	C <sub>18</sub> H <sub>34</sub> O <sub>2</sub>
Ethyl acetoacetate	C <sub>6</sub> H <sub>10</sub> O <sub>3</sub>	Polyethylene glycol 200	C <sub>2</sub> H <sub>4</sub> O
Glycerol	C <sub>3</sub> H <sub>8</sub> O <sub>3</sub>	Silicone oil Siluron 5000	C <sub>2</sub> H <sub>6</sub> O <i>Si</i>
Potassium Chloride 4.01%	KCl H <sub>2</sub> O	Potassium Chloride 7.71%	KCl H <sub>2</sub> O
Potassium Chloride 11.13%	KCl H <sub>2</sub> O	Potassium Chloride 20.03%	KCl H <sub>2</sub> O
Carbon graphite	C	UHMWPE	(C <sub>2</sub> H <sub>4</sub> ) <sub>n</sub>
Polypropylene	(C <sub>3</sub> H <sub>6</sub> ) <sub>n</sub>	Nylon 6.6-101	(C <sub>12</sub> H <sub>22</sub> N <sub>2</sub> O <sub>2</sub> ) <sub>n</sub>
PMMA	(C <sub>5</sub> H <sub>8</sub> O <sub>2</sub> ) <sub>n</sub>	Polycarbonate	(C <sub>16</sub> H <sub>14</sub> O <sub>3</sub> ) <sub>n</sub>
Teflon	(C <sub>2</sub> F <sub>4</sub> ) <sub>n</sub>	Al <sub>2</sub> O <sub>3</sub> 99.7%	Al <sub>2</sub> O <sub>3</sub>
Water	H <sub>2</sub> O		

Now the true stopping powers are calculated with given data for all the sample materials. Then the estimation of the effective atomic number is calculated for DECT and all the windows of spectral CT for LN450, AP6, SB3, carbon and Al<sub>2</sub>O<sub>3</sub>. With this effective atomic number the mean excitation energy is calculated and also plotted against the separation. With the mean excitation energy the stopping power is calculated. Then finally the true stopping powers are plotted in the same graph as the stopping power of DECT and the stopping powers of every window of spectral CT. Then the relation between the stopping powers estimated by DECT and by spectral CT is shown, especially how the different windows of spectral CT influence the stopping power.

## 4 Results

### 4.1 HU Values

The HU values are calculated using equation 4 then the  $HU_{high}/HU_{low}$  is plotted against the separation. This gave the following results as can be seen in figure 9, the relation is shown for CB2-50, carbon and nylon. These sample materials were chosen, because they represent some typical results. For some of the materials the  $HU_{high}/HU_{low}$  became smaller for a bigger separation, sometimes it became bigger and sometimes it had a strange jump in the values. This could be explained by the fact that sometimes the HU value is a negative number, so when both  $HU_{high}$  and  $HU_{low}$  are negative the absolute value of both values goes up but when the minus cancel each other out the value after dividing goes down. This also explained the strange jumps, because then one of the HU values would become negative.

### 4.2 Linear attenuation coefficient

The linear attenuation coefficient is calculated using formula 5, then the values of  $\mu_{high}/\mu_{low}$  are calculated and plotted against the separation. This gave the data shown in figure 10. All the plots looked the same way for all the materials, this can be explained by the fact that value of  $\mu_{high}$  increases for the narrowing window, while  $\mu_{low}$  decreases for the narrowing window. When looking again at figure 6 it can be seen why. When the high energy spectrum moves to the right the average energy becomes bigger, when the low energy spectrum moves to the left the average energy becomes smaller. Therefore  $\mu_{high}/\mu_{low}$  is becoming bigger. In figure 11 the same spectrum is plotted as in figure 6 only now with the last window drawn.

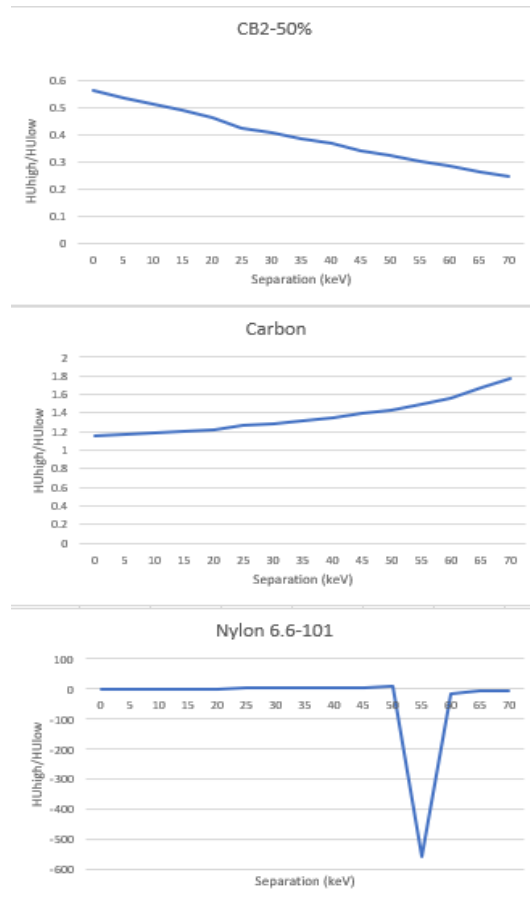


Figure 9:  $HU_{high}/HU_{low}$  vs separation for CB2-50%, carbon and nylon 6.6-101.

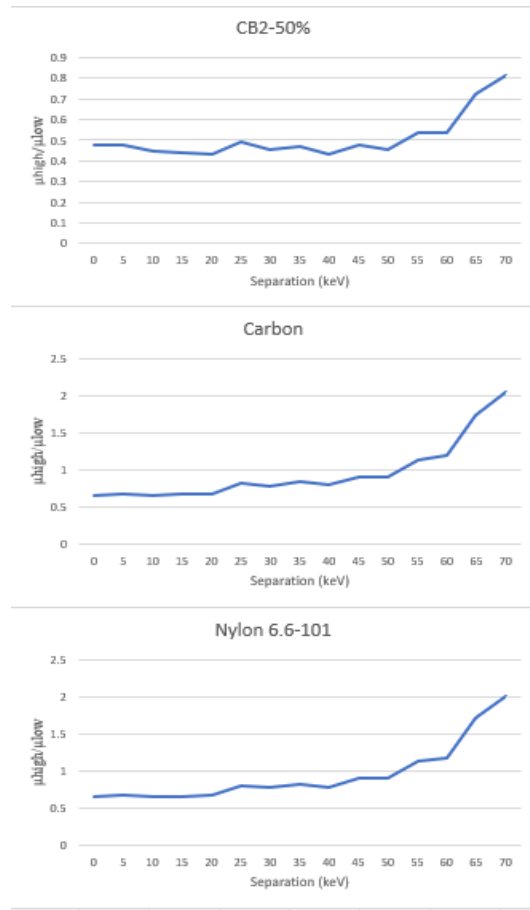


Figure 10:  $\mu_{high}/\mu_{low}$  vs Separation for CB2-50%, carbon and nylon 6.6-101.

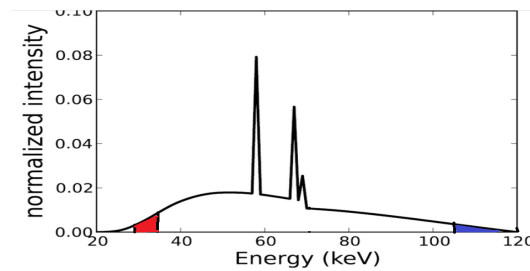


Figure 11: Spectral CT with a tube voltage of 120keV and two channels ranging from [30,35]keV and [105,120]keV. The high energy window is drawn in blue, the low energy window is drawn in red[13].

### 4.3 True stopping power

The true stopping power is calculated for all 39 sample materials using formula 6, formula 7 and formula 8. The data for the true stopping power is shown in figure 12. It can be seen that more denser materials have relatively bigger stopping powers than less denser materials. Also it is shown that for all materials the protons are stopped in several centimeters which is what was expected.

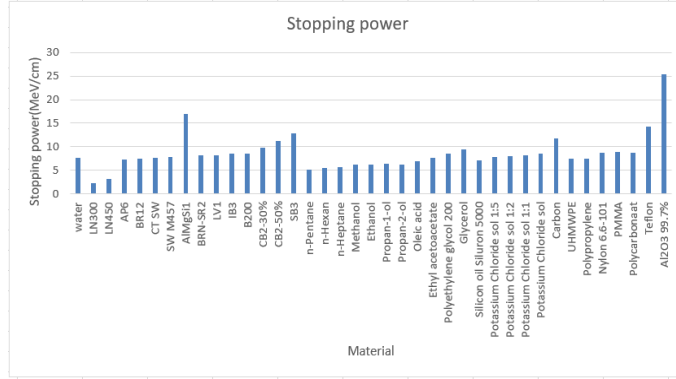


Figure 12: Stopping power in MeV/cm for 39 different sample materials

### 4.4 Effective atomic number

With the data acquired from the DECT and spectral CT the effective atomic number, electron density and the  $\mu_{high}/\mu_{low}$  are calculated for 5 different materials. The tissue materials are plastics which behave the same in a CT as the tissues they represent. This is done for LN450, AP6, SB3, carbon and  $Al_2O_3$ . LN450 represents a piece of lung, AP6 represents an adipose, SB3 represents a cortical bone, carbon is carbon and  $Al_2O_3$  is aluminum-oxide. The effective atomic number is calculated with formula 11 for DECT and for every set of window of spectral CT. This is then plotted against the window separation relative to a separation of 0. Also the electron density and the  $\mu_{high}/\mu_{low}$  is plotted relative to a separation of 0. This is done by using formula 12

$$F(E) = \frac{F(S) - F(0)}{F(0)} * 100\% \quad (12)$$

F is here the function which is going to be expressed relative to a separation of zero, all function which are expressed relative to a separation of zero are calculated with this equation. As can be seen in the figure 13 till figure 17 the effective atomic number Z' goes down when the window separation becomes longer. This is due to the fact that  $\mu_{high}/\mu_{low}$  is decreasing for a bigger separation. For  $\mu_{high}/\mu_{low}$  we see the same form of graph as before which is what was expected. The electron density differs a bit per material, this is due to

the fact that the electron density depends on a lot of material properties. The separation ranges till  $S=65\text{keV}$  for SB3 and  $\text{Al}_2\text{O}_3$ , due to the fact that there were some numerical errors in the system weighting functions for such a big separation. Therefore the values of  $S=70\text{keV}$  are ignored from now on for these sample materials in the results.

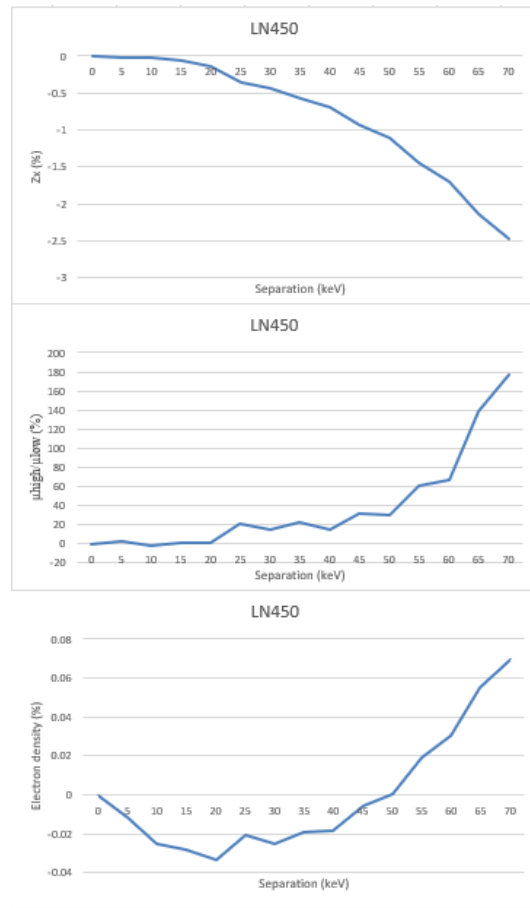


Figure 13: Effective atomic number,  $\mu_{high}/\mu_{low}$  and the electron density relative to zero separation in percentage vs the separation for LN450.

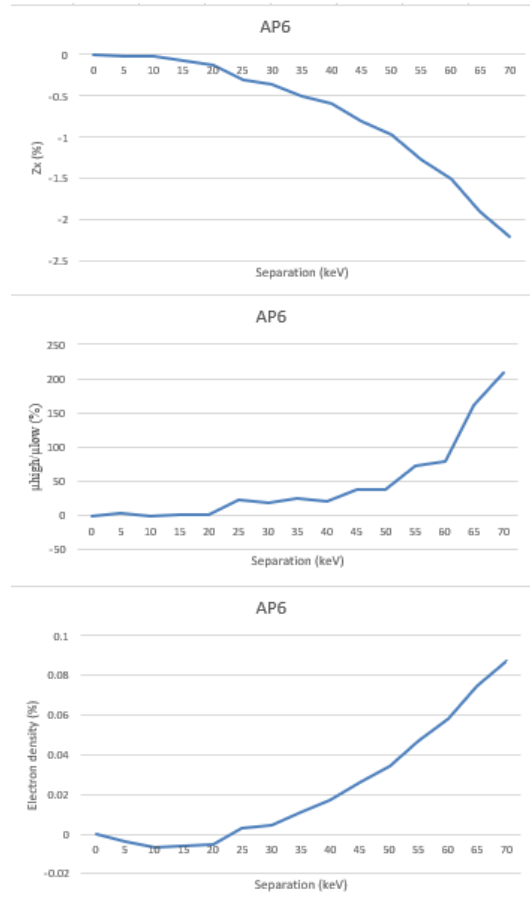


Figure 14: Effective atomic number,  $\mu_{high}/\mu_{low}$  and the electron density relative to zero separation in percentage vs the separation for AP6.

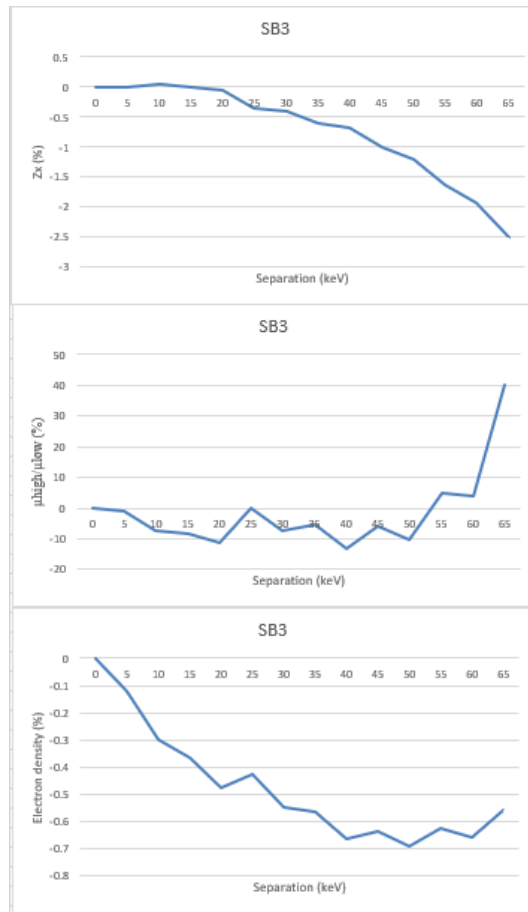


Figure 15: Effective atomic number,  $\mu_{high}/\mu_{low}$  and the electron density relative to zero separation in percentage vs the separation for SB3.

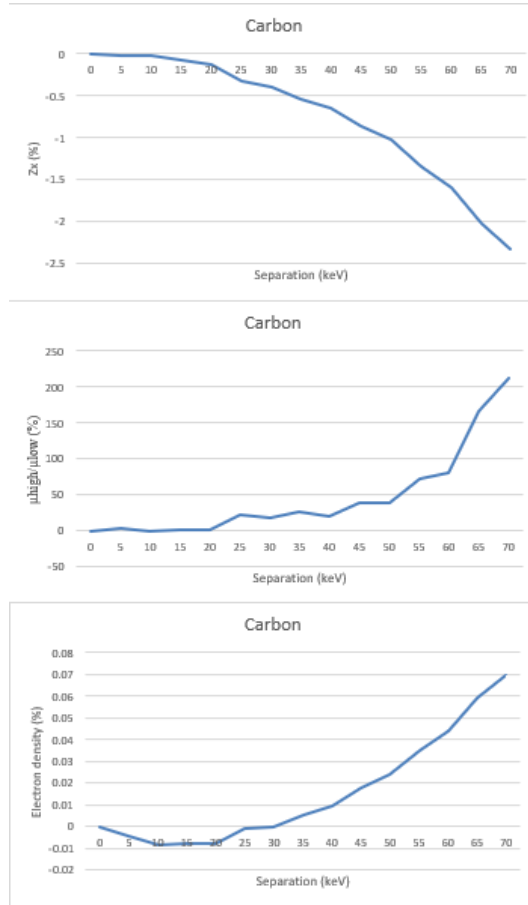


Figure 16: Effective atomic number,  $\mu_{high}/\mu_{low}$  and the electron density relative to zero separation in percentage vs the separation for carbon.

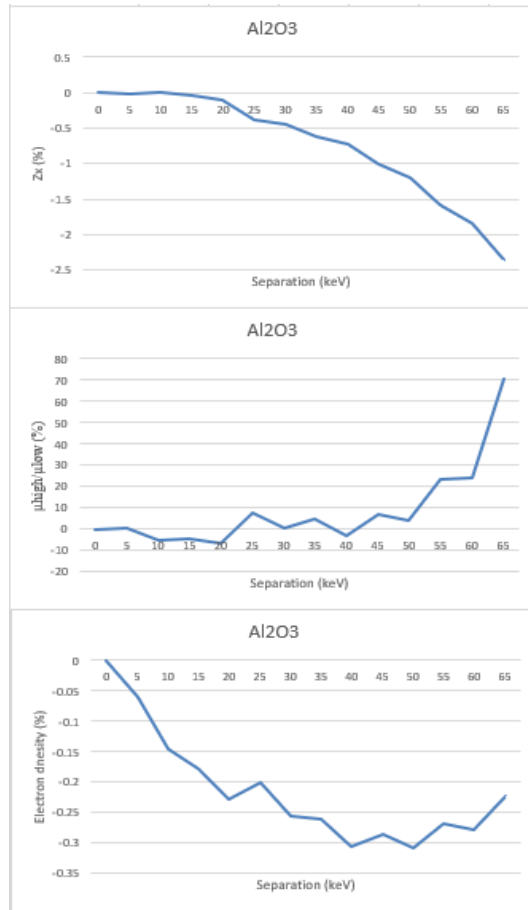


Figure 17: Effective atomic number,  $\mu_{high}/\mu_{low}$  and the electron density relative to zero separation in percentage vs the separation for  $\text{Al}_2\text{O}_3$ .

## 4.5 Mean excitation energy

The mean excitation energy is calculated using formula 11, the mean excitation energy relative to a separation of zero is plotted against the separation for the 5 sample materials used and is shown in figure 18. It can be seen that the mean excitation energy goes down for a bigger separation, this is due to the fact that also the effective atomic number  $Z'$  decreases.

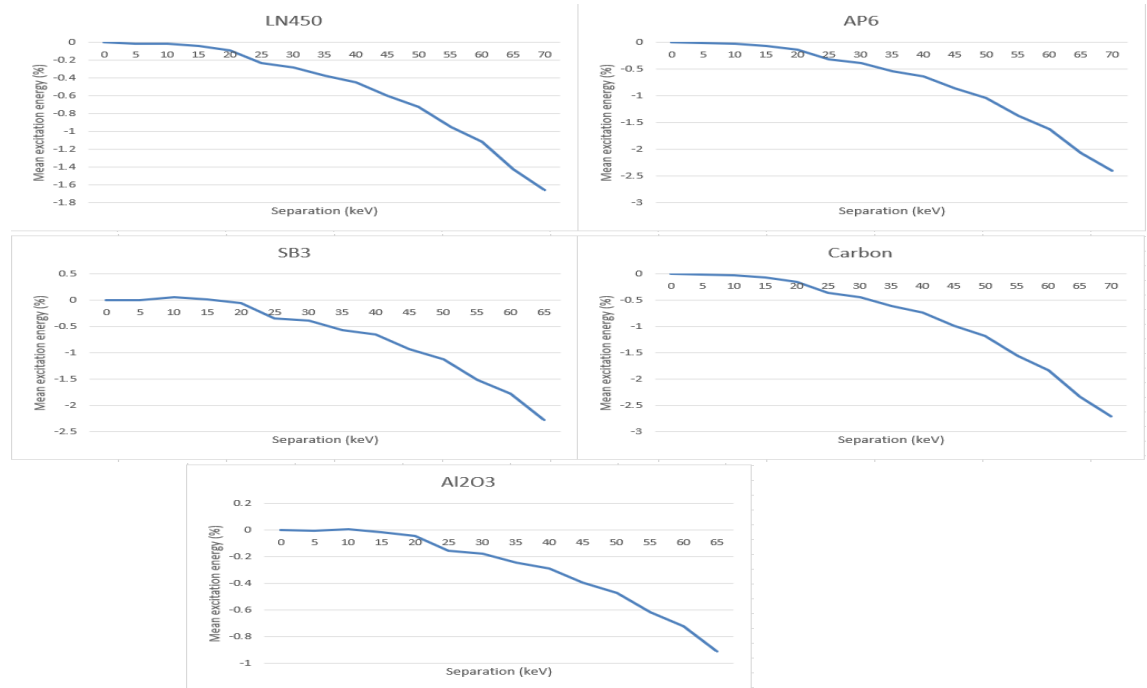


Figure 18: Mean excitation energy relative to a separation of zero vs the separation for LN450, AP6, SB3, carbon and  $\text{Al}_2\text{O}_3$ .

## 4.6 Stopping power

The stopping power is calculated with the mean excitation energy using formula 6. The stopping power is plotted for every window of spectral CT relative to the true stopping power using formula 13

$$S = \frac{S_{ct} - S_{true}}{S_{true}} * 100\% \quad (13)$$

Also the values for dual energy CT are plotted relative to the true stopping power at every separation for clarity, dual energy CT does not use this window but is just one fixed value plotted at every separation. The stopping power of LN450 is shown in figure 19. It can be seen that for the bigger separations the stopping power comes closer to zero which would mean it is equal to the true stopping power. The estimation of spectral CT becomes a better estimation after a separation of 65keV, however both values are close to the true stopping power.

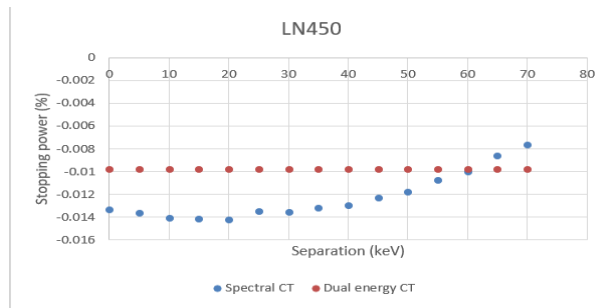


Figure 19: Stopping power relative to the true stopping power vs separation plotted for spectral CT and dual energy CT for LN450. Dual energy CT is plotted multiple times for clarity.

The stopping power of AP6 is plotted in figure 20, it can be seen that for LN450 spectral CT gives a better estimation for the lower separations. Dual energy CT becomes a better choice after the separation exceeds a separation of 45keV. All though again when looking at the percentage on the y-axis it can be seen that both choices give a good estimation. The stopping power of SB3 is plotted in figure 21, for SB3 the estimation of the stopping power of spectral CT changes almost to nothing for the different separations. Dual energy CT is the better choice for the estimation of stopping powers for SB3. The stopping power of Carbon is plotted in figure 22, for Carbon the low separation windows give a better estimation of the stopping power than dual energy CT. After a separation of 40keV dual energy CT becomes a better choice. The stopping power of  $Al_2O_3$  is plotted in figure 23, for  $Al_2O_3$  there is also little variation in the estimated stopping power for the different windows of spectral CT. The estimation of Dual energy CT gives a better approximation of the stopping power than spectral CT.

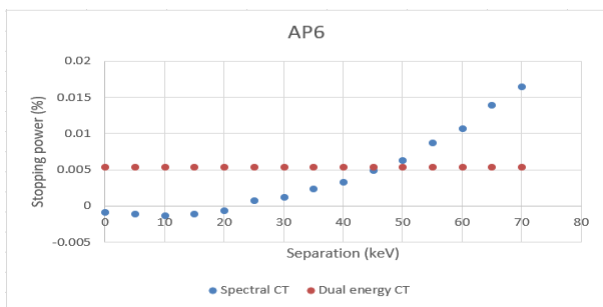


Figure 20: Stopping power relative to the true stopping power vs separation plotted for spectral CT and dual energy CT for AP6. Dual energy CT is plotted multiple times for clarity.

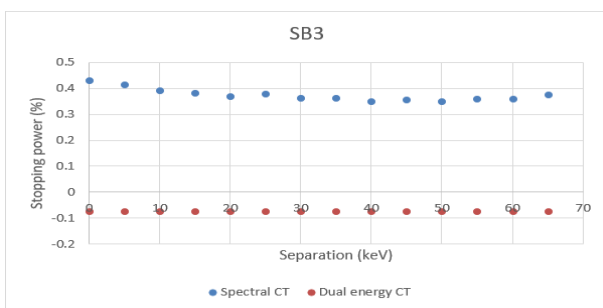


Figure 21: Stopping power relative to the true stopping power vs separation plotted for spectral CT and dual energy CT for SB3. Dual energy CT is plotted multiple times for clarity.

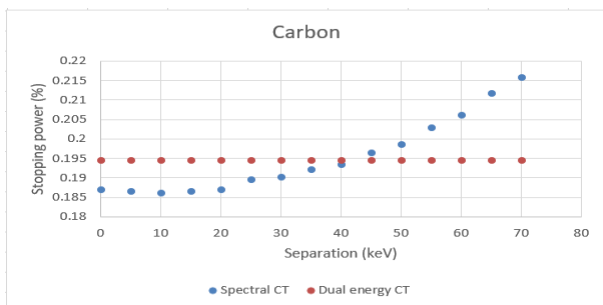


Figure 22: Stopping power relative to the true stopping power vs separation plotted for spectral CT and dual energy CT for Carbon. Dual energy CT is plotted multiple times for clarity.

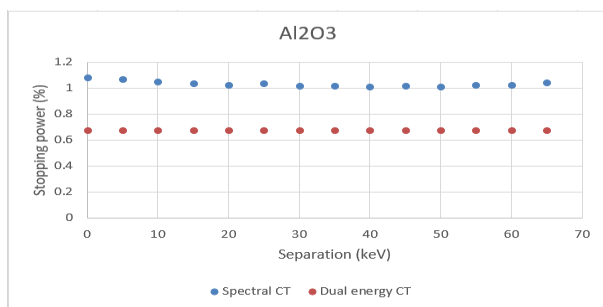


Figure 23: Stopping power relative to the true stopping power vs separation plotted for spectral CT and dual energy CT for  $\text{Al}_2\text{O}_3$ . Dual energy CT is plotted multiple times for clarity.

## 5 Discussion and conclusion

The true stopping power of 39 materials are calculated, then 5 materials are chosen and their stopping power is calculated by dual energy CT and by two channel spectral CT for different windows to see which gives a better estimation. It is dependent on the material which CT scan gives a better estimation of the stopping power, however both the dual CT and every window of choice of spectral CT gives an estimation within approximately 1% of the true stopping power. There is some indication that for the heavier materials the window variations of spectral CT has almost no effect on the estimation of the stopping power, however to really draw this conclusion this research must be expanded for far more materials. Also the X-ray tube voltage of both the dual CT as well as the spectral CT can be varied to see how this influences the estimation. The proton energy is chosen to be 219MeV, which could also be changed to see how the proton energy would influence the estimations of the stopping power. The different width of the windows can also be expanded to include more windows and for example see what would happen if 3 or more channels would be introduced. Both the dual CT and every window of spectral CT give estimations of the stopping power very close to the true stopping power, therefore it might be more interesting to see what the dose is of these CT scans and see how this dose can be reduced.

## References

- [1] R. A. Amos, "Proton and carbon ion therapy.," *Medical physics*, vol. 40, no. 5, 2013.
- [2] G. Ising, "Prinzip einer methode zur herstellung von kanalstrahlen hoher voltzahl," *Ark. Mat. Astron. Fys.*, vol. 18, pp. 1-4, 1924.

- [3] W. Levin, H. Kooy, J. Loeffler, and T. DeLaney, "Proton beam therapy," *British journal of Cancer*, vol. 93, no. 8, p. 849, 2005.
- [4] L. Saba, M. Porcu, B. Schmidt, and T. Flohr, "Dual energy ct: basic principles," in *Dual energy CT in oncology*, pp. 1–20, Springer, 2015.
- [5] R. Behling, *Modern diagnostic x-ray sources: technology, manufacturing, reliability*. CRC Press, 2015.
- [6] A. D. McNaught and A. D. McNaught, *Compendium of chemical terminology*, vol. 1669. Blackwell Science Oxford, 1997.
- [7] T. G. Feeman, "The mathematics of medical imaging," *Sringer*,, 2010.
- [8] M. B. of Science in Medical Imaging, "Hu values - ct abdomen/pelvis," 2016.
- [9] T. R. Johnson, "Dual-energy ct: general principles," *American Journal of Roentgenology*, vol. 199, no. 5\_supplement, pp. S3–S8, 2012.
- [10] S. Faby, S. Kuchenbecker, S. Sawall, D. Simons, H.-P. Schlemmer, M. Lell, and M. Kachelrieß, "Performance of today's dual energy ct and future multi energy ct in virtual non-contrast imaging and in iodine quantification: A simulation study," *Medical physics*, vol. 42, no. 7, pp. 4349–4366, 2015.
- [11] R. F. Barber, E. Y. Sidky, T. G. Schmidt, and X. Pan, "An algorithm for constrained one-step inversion of spectral ct data," *Physics in Medicine & Biology*, vol. 61, no. 10, p. 3784, 2016.
- [12] P. Coan, A. Bravin, and G. Tromba, "Phase-contrast x-ray imaging of the breast: recent developments towards clinics," *Journal of Physics D: Applied Physics*, vol. 46, no. 49, p. 494007, 2013.
- [13] J. K. van Abbema, *Accurate Relative Stopping Power Prediction from Dual Energy CT for Proton Therapy: Methodology and Experimental Validation*. Rijksuniversiteit Groningen, 2017.
- [14] J. E. Turner, "Atoms, radiation, and radiation protection," *Atoms, Radiation, and Radiation Protection, 2nd Edition, by James E. Turner, pp. 576. ISBN 0-471-59581-0. Wiley-VCH, April 1995.*, p. 576, 1995.
- [15] M. N. Sarsam *et al.*, "Stopping power for proton interacting with aluminum, beryllium and carbon using different formulas," *Al-Qadisiyah Journal Of Pure Science*, vol. 18, no. 1, pp. 135–144, 2017.
- [16] H. Woodard and D. White, "The composition of body tissues," *The British journal of radiology*, vol. 59, no. 708, pp. 1209–1218, 1986.